Materials Research. 2017; 20(6): 1461-1469
DOI: http://dx.doi.org/10.1590/1980-5373-MR-2016-1064

Influence of Aluminum Addition in the Framework of MCM-41 Mesoporous Molecular Sieve Synthesized by Non-Hydrothermal Method in an Alkali-Free System

Nathália La-Salvia[a]*, Juan José Lovón-Quintana[a], Adriana Siviero Pagani Lovón[a], Gustavo Paim Valença[a]

[a]Laboratório para o Estudo de Processos de Adsorção e Catálise - LEPAC, Faculdade de Engenharia Química, Universidade Estadual de Campinas - UNICAMP, Cidade Universitária Zeferino Vaz, Av. Albert Einstein, 500, 13083-852, Campinas, SP, Brasil.

Received: December 12, 2016; Revised: June 01, 2017; Accepted: July 21, 2017

Purely siliceous MCM-41 and Al-containing MCM-41 (Al-MCM-41) mesoporous materials were synthesized by non-hydrothermal method in alkali-free ions medium at room temperature and short reaction times. Under these synthesis conditions, it was also investigated the influence of Al incorporation in the crystal structure of MCM-41. The solids were characterized by ICP-OES, AAS, N_2 adsorption at 77 K, XRD, TEM, NH_3-TPD, ^{27}Al and ^{29}Si-MAS-NMR, FT-IR and TGA. The resulting mesoporous materials showed a well-defined hexagonally ordered pore geometry maintaining a uniform and unimodal pore size distribution with high specific surface areas (1000-1400 m^2g^{-1}). The Al^{+3} ions were introduced successfully in the structure of the purely siliceous MCM-41 expanding the unit cell parameter and forming four-coordinated Al species, and in a less extent, forming six-coordinated Al species. In addition, the surface acidity of the MCM-41 increased with Al loading. Contrary, the presence of Al in the MCM-41 mesoporous structure resulted in a decrease of the crystallinity and specific surface area possibly due to the presence of Al species in highly distorted tetrahedral structures and Al extra-framework or amorphous alumina occluded in the pores. The MCM-41 type mesoporous materials obtained in this work show similar characteristics of those synthesized by conventional hydrothermal methods.

Keywords: *MCM-41, Al-MCM-41, non-hydrothermal method, alkali-free system.*

1. Introduction

Purely siliceous MCM-41, a member of the M41S family synthesized by Mobil Oil Corporation, has unique properties such as high surface area that may reach up to 1600 m^2g^{-1}, well-ordered and uniform cylindrical mesoporous arrangement with pore size from 2 to 10 nm, and good thermal stability[1-3]. However, the purely siliceous MCM-41 has a neutral framework showing weak surface acidity, limiting its potential commercial applications mainly as a catalyst in petrochemical industry and production of fine and specialty chemicals as well as in selective adsorption process widely used in separation operations and environmental control[4,5]. One possibility of tuning their framework properties and surface reactivity is through incorporation of different cations (e.g., Al^{3+}, Fe^{3+}, Ga^{+3}, B^{+3}) in the structure of the MCM-41 by isomorphic substitution or by post-synthesis impregnation[6]. Therefore, Al-containing MCM-41 (Al-MCM-41) is one of the most studied mesoporous materials due to the nature of its acid sites, in particular the BrØnsted ones, produced by incorporation of the tetrahedrally coordinated aluminum to the framework of MCM-41 widely used in organic chemical reactions[4,5].

In the current state of art, the synthesis of MCM-41 and Al-MCM-41 mesoporous materials, as shown in Table 1, it can be achieved by using a broad spectrum of silica and aluminum precursors, surfactant templates and pH adjustments in a wide range of reactional molar compositions, synthesis conditions, and thermal or chemical processes for removal of surfactants. Usually the MCM-41 type materials are obtaining by hydrothermal techniques in alkali ions medium (ions Na^+) at temperatures in the range of 343 - 423 K and after drying, the solids are calcined in air flow at 813 or 823 K from 5 to 12 hours for surfactants removal. These synthesis procedures usually take 1 or 2 days or even longer and are quite disadvantageous for their production in large-scale. In addition, the presence of alkali metal ions (ions Na^+) in the mesoporous structure may bring some limitations such as structural instability in processes that involve high temperature steam streams[7] and in some specific applications (e.g., catalysis) inhibiting the surface activity of the solids[5]. Moreover, previous studies have shown that in the synthesis of MCM-41 at room temperature with sodium ions medium leads to poor condensation of the silica groups, resulting in structures thermally less stable than those synthesized in high temperatures[4].

*e-mail: nathalialasalvia@gmail.com

Table 1. Synthesis methods of MCM-41 type mesoporous materials

Ref.	Precursors Si	Precursors Al	Basic medium	Surfactant templates	Reaction SM:T(K)/time	Calcination T(K)/time	Si/Al	d_{100} (nm)	a_0 (nm)	S_{BET} (m^2g^{-1})	V_p (cm^3g^{-1})	D_p (nm)	W_t (nm)
In an alkali-free system													
[8]	TEOS+MPTMOS		NH_3-H_2O-C_2H_5OH	CTAB	NH:338/1h	673/5h	∞	3.1	3.5	1621	0.69	2.6	*0.90*
	TEOS+MPTMOS			CTAB+TMB			∞	3.8	4.4	1308	1.03	3.5	*0.90*
[12]	Fumed silica		NH_4OH+TMAOH	CTAB	H:343/3d	813/5h	∞	3.72	4.3	1040	0.97	3.44	0.86
[13]	Colloidal silica		TMAOH	CTAB	H:373/2d	823/12h	∞	*3.99*	4.16	1154	0.84	3.4	0.76
[14]	TEOS		NH_4OH	CTAB	H:383/2d	823/6h	∞	3.04	3.51	1082	0.97	2.53	0.98
[15]	Fumed silica		NH_4OH	CTAB	H:373/3d	550/24h	∞			1126		2.98	
[9]	TEOS	AIP + PrOH	NH_4OH	CTAB	NH:RT/0.5h	823/5h	61			1020	0.57	2.2	
							13			950	0.48	2.0	
[10]	TEOS	AIP	NH_4OH	C16TMABr-PrOH	NH:RT/1h	823/11h	101	*3.73*	4.31	1034	0.77	3.08	*1.23*
		Aluminum sulfate		C16TMABr			27	*3.67*	4.24	988	0.72	2.99	*1.25*
[15]	Fumed silica	Aluminum sulfate	NH_4OH	CTAB	H:373/3d	550/24h	14			997		2.9	
[10]	Fumed silica + TMASi	Alumina	NH_4OH	C16TMACl	H:377/2d	823/11h	32	*4.04*	4.67	889	0.71	3.61	*1.06*
					H:423/2d		23	*4.71*	5.44	811	0.73	3.88	*1.66*
In an alkali system													
[11]	TEOS		NaOH	CTAB	NH:RT/36h	823/6h	∞			1230	0.77	3.38	
[16]	Silica gel		NaOH	CTAB	H:373/1h	813/5h*	∞	4.0	*4.61*	610	1.4	2.7	*1.92*
					H:373/2h		∞	4.2	*4.85*	1270	2.0	2.5	*2.35*
[17]	TEOS		NaOH	CTAB	H:373/8d	773/6h*	∞	*3.65*	4.22	1182			
[10]	TEOS	Sodium aluminate	NH_4OH	C16TMABr	NH:RT/1h	823/11h	32	*3.75*	4.33	977	0.71	3.00	*1.33*
[11]	TEOS	AIP	NaOH	CTAB	NH:RT/36h	823/3h	20.5			1156	0.76	3.38	
							4.7			450	0.48	3.37	
[18]	Fumed silica + TMASi + sodium silicate	AIP		CTAB	H:373/1d	823/5h*	50	3.74	*4.32*	1147		2.76	*1.56*
		Pseudo boehmite					50	3.29	*3.80*	1010		2.19	*1.61*
		Aluminum sulfate					50	3.56	*4.11*	834		2.54	*1.57*
[13]	Colloidal silica	Sodium aluminate	TMAOH	CTAB	H:373/2d	823/12h	12.5	*3.80*	4.39	983	0.76	3.56	0.84
[19]	TEOS	Sodium aluminate	NaOH	CTAB	H:373/6d	773/6h*	100	*3.84*	4.43	1203			
							10	*3.88*	4.48	1161			
[10]	Colloidal silica + TMASi	Sodium aluminate	NH_4OH+TMAOH	C16TMACl	H:377/2d	823/11h	18	*3.80*	4.39	1020	0.82	3.45	*0.94*

Numeric data in italics: estimated values. d_{100}, d-spacing value; a_o unit cell parameter; S_{BET}, BET specific surface area; V_p, total pore volume; D_p, pore diameter; W_t, pore wall-thickness; SM, synthesis method; H, hydrothermal synthesis in autoclave at high vapor pressure; NH, non-hydrothermal synthesis; RT: room temperature; d: day; h: hour. AIP: aluminum isopropoxide; C16TMABr: hexadecyltrimethylammonium bromide; C16TMACl: hexadecyl-trimethyl-ammonium chloride; CTAB: cetyltrimethylammonium bromide; MPTMOS: 3-methacryloxypropyltrimethoxysilane; PrOH: propan-2-ol; TEOS: tetraethyl orthosilicate; TMASi: tetramethylammonium silicate; TMAOH: tetramethylammonium hydroxide; TMB: 1,3,5-trimethylbenzene; * samples were previously pretreated in inert gas flow at the same calcination temperature.

On the other hand, in the literature was also proposed to obtain well-structured MCM-41 and Al-MCM-41 mesoporous materials by hydrolysis and condensation-copolymerization reactions of Si and Al organometallic compounds, also known as non-hydrothermal synthesis[8-11]. In spite of the simplicity of the non-hydrothermal synthesis techniques, little has so far been published, there being more information about the influence of different metal sources in the textural properties of the MCM-41 type mesoporous materials and scarce information about the rearrangement of the crystalline structure and the nature of the surface activity (e.g., acid sites) as a consequence of the incorporation of heteroelements in the framework of MCM-41 mesoporous materials.

In order to overcome some of the limitations mentioned above, the main goal of our study was to propose the synthesis of a purely siliceous MCM-41 and Al-containing MCM-41 (Al-MCM-41) mesoporous materials by non-hydrothermal economically feasible procedures using a simple alkali-free reaction system carried out at room temperature and short reaction times. Under these synthesis conditions, aiming to elucidate the intrinsic structural properties and active nature of mesoporous silica based materials, it was also investigated the increasing influence of Al incorporation in the changes of the textural properties, crystalline structure and active nature (acid sites) of the MCM-41 without interferents (e.g., Na^+ ions). The technical data reported in this study are of great importance because validate an alternative technique for obtaining MCM-41 and Al-MCM-41 mesoporous materials, the same that are commonly obtained by hydrothermal methods, besides that these results constitute a basis for the development of new materials for specific applications such as in catalysis and adsorption.

2. Experimental

2.1 Synthesis

Purely siliceous MCM-41 and Al-containing samples with Si/Al molar ratios of 50 and 15 named Al-MCM-41(50) and Al-MCM-41(15), respectively, were synthesized according to the procedure described previously[20]. Briefly, a solution with 630 cm^3 ammonium solution - NH_4OH (Merck, 26,4%) and 810 cm^3 of deionized water was prepared. To this mixture 6 g of cetyltrimethylammonium bromide, $C_{19}H_{42}BrN$ - CTAB (Sigma Aldrich, 99%) and 0.5 g (Si/Al = 50) or 1.7 g (Si/Al=15) of aluminum sulfate hydrate, $Al_2(SO_4)_3.18H_2O$ (Merck, 59%) were added. After solubilization, 30 cm^3 of tetraethyl orthosilicate, $SiC_8H_{20}O_4$ - TEOS (Sigma Aldrich, 98%) was added. The resulting suspension was stirred at 420 rpm for 2 h, at room temperature, having the following molar composition ratios 1Si[TEOS]: 0.12CTAB: $31NH_4OH$: $338H_2O$: xAl[$Al_2(SO_4)_3.18H_2O$], where x = 0, 0.013 and 0.044 for pure silica, Si/Al=50 and Si/Al=15 samples, respectively. Afterwards, the material was filtered and dried overnight at 400 K. The sample was then calcined at 813 K for 11 h. The first 5 h in a nitrogen flow and the remaining time in a synthetic air flow. Finally, the resulting product was cooled to room temperature under continuous synthetic air flow and stored in a desiccator.

2.2 Characterization

The total silica content was determined in an Atomic Absorption Spectroscopy (AAS) of Perkin Elmer (AAnalyst 3) and the aluminum loading in a Perkin-Elmer spectrometer (Elan DRC-e). Powder X-ray diffraction (XRD) patterns were carried out in a Philips (X'Pert) X-ray diffractometer using $CuK\alpha_1$ radiation (λ = 0.154056 nm) at 40 kV and 40 mA, in the range of 2θ from 1.8º to 15º with a step size of 0.02º and a time step of 1.8 s. Prior to the XRD analysis, the samples were dried at 393 K overnight and powdered. The d-spacing value (d_{100}) was estimated from the position of the first X-ray diffraction line using the Bragg's equation ($2d_{100}sin\theta = n\lambda$) and the unit cell parameter (a_0) for a hexagonal lattice from the equation $a_0 = 2d_{100}/\sqrt{3}$. The specific surface area, the pore size distribution and the total pore volume were determined from N_2 adsorption-desorption isotherms obtained at 77 K in a Micromeritics ASAP 2020 analyzer. The samples (ca. 100 mg) were previously heated under vacuum and degassed at 623 K for 1 h. The surface area was calculated by the conventional BET method in the relative pressure range $0.05 < P/P_o < 0.20$ with a linear correlation coefficient greater than 0.999. The total pore volume (V_p) was measured by the amount of N_2 adsorbed at a relative pressure close to one ($P/P_0 \approx 0.995$). The average pore diameter (D_p) was determined by BJH method from the N_2 desorption isotherms. Then, the pore wall-thickness (W_t) was estimated by the equation $W_t = a_0 - D_p$. The morphological properties of samples were investigated by Transmission Electron Microscopy (TEM) in a FEI Titan Microscopy with an accelerating voltage of 300 kV.

The Al and Si structural species were determined from ^{27}Al-MAS-NMR and ^{29}Si-MAS-NMR spectra using a Bruker (AC400/P) spectrometer. The distribution of the tetrahedral and octahedral aluminum structures was determined with a resonance frequency of 104,3 MHz and 1 µs pulse length. ^{27}Al chemical shifts were measured relative to triaquatrihydroxyaluminium complex ion - $[Al(H_2O)_6]^{3+}$. ^{29}Si-MAS-NMR measurements were based on the single-contact cross-polarization method at 79.4 MHz with a pulse length of 4 µs using tetramethylsilane - $Si(CH_3)_4$ as reference. Surface acidity was determined by NH_3-TPD method using a Micromeritics Auto Chem II 2920 coupled to a mass spectrometer MKS (Cirrus LM99). The samples (ca. 150 mg) were pretreat in helium flow (50 cm^3min^{-1}) at 773 K for 60 min. Afterwards cooled at 353 K and saturated with ammonia (15%NH_3/helium) by a total of 10 pulses (loop volume: 0.5 cm^3). Then, the reactor temperature was raised up to 473 K, purged with helium during 30 min and

ramped up to 1123 K at a rate of 10 K min^{-1} in continuous helium flow. The functional groups present on surface of the solids were determined by Fourier transform infrared spectroscopy (FT-IR) in an equipment of Thermo Scientific (Nicolet 6700) spectrometer. Prior to FT-IR analysis the samples were heated at 393 K overnight, milled and mixed with spectroscopic grade potassium bromide (KBr) in a ratio of ≈1:10. The powder was pressed up to 15 kg cm^{-2} for 10 min to form transparent wafers. The measurements were obtained in the transmittance mode from 400 to 4000 cm^{-1} with 64 scans and a resolution of 4 cm^{-1}.

In order to investigate the complete removal of the structure-directing agent, Thermogravimetric Analysis (TGA) was carried out in a TA Instrument (2050). The sample (ca. 10 mg) as-synthesized was placed in a platinum pan and heated from room temperature to 973 K in a rate of 10 K min^{-1}, under a continuous synthetic air flow (10 mL min^{-1}).

3. Results and Discussions

Figures 1 and 2 show the low-angle X-ray powder diffraction patterns and N_2 adsorption-desorption isotherms with pore-size distribution graphs inset of purely siliceous MCM-41 and Al-containing samples Al-MCM-41 calcined at 813 K. In Table 2 are summarized the chemical compositions, structural parameters and textural properties of the solids.

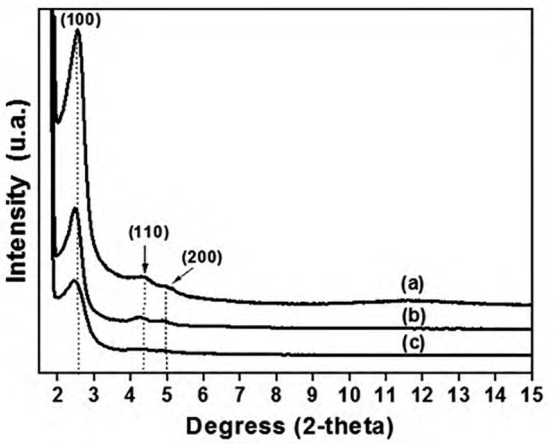

Figure 1. XRD patterns of samples of **(a)** MCM-41, **(b)** Al-MCM-41(50), **(c)** Al-MCM-41(15).

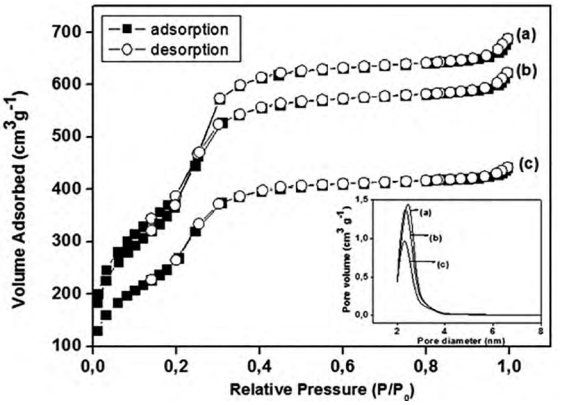

Figure 2. N_2 adsorption-desorption isotherms at 77K and BHJ pore size distribution curves of **(a)** MCM-41, **(b)** Al-MCM-41(50), **(c)** Al-MCM-41(15).

The XRD patterns of all samples exhibit a very strong and well-resolved peak at 2Θ = 2.5° assigned to the reflection line (100), and very weak and broad two peaks at 2Θ = 4.3° and 4.9°, corresponding to the reflections lines (110) and (200), respectively. The intense reflection line (100) is characteristic of the hexagonal structure (space group p6mm) of the purely siliceous MCM-41 (ICDD#49-1712) and the presence of the reflection lines (110) and (200) confirm the highly crystallinity and the well-defined hexagonally ordered pore geometry of the mesoporous materials[1-3,13]. However, when Al was incorporated in the purely siliceous MCM-41 the main reflection line (100) became broader and less intense, even at very low levels of aluminum content, and the reflection lines (110) and (200) are hardly observed. Furthermore, with the rise of aluminum content or decrease of the Si/Al ratio, the d-spacing values (d_{100}) increased and, consequently, the unit cell parameters (a_0) expanded (Table 2). The increase of the interplanar spacing suggests that aluminum was incorporated into the structure of MCM-41 and this could be due to the difference in size between aluminum ions, Al^{+3} (radius = 53 pm) and silicon ions, Si^{+4} (radius = 40 pm)[13,18,21]. The latter are in agreement with the literature, and independent of the synthesis method, it is commonly accepted that the incorporation of Al^{+3} ions in the MCM-41 structure produce an expansion on its crystalline reticulum causing a narrowing of the pore size and a decrease in the crystallinity degree of the mesoporous materials[13,18,19,21,22].

Table 2. Physicochemical properties of the calcined solids.

Samples	Si content (wt%)		Al content (wt%)		d_{100} (nm)	a_0 (nm)	S_{BET} (m^2g^{-1})	V_p (cm^3g^{-1})	D_p (nm)	C_{BET}	W_t (nm)	Acid sitesdensity (mmol g^{-1})
	as-synthesized	calcined	as-synthesized	calcined								
MCM-41	46.74	46.60	-	-	3.48	4.02	1412	1.06	2.65	59	1.37	0.06
Al-MCM-41(50)	45.96	45.35	0.88	0.87	3.56	4.12	1390	0.97	2.61	51	1.51	0.36
Al-MCM-41(15)	44.24	44.25	2.83	2.74	3.62	4.19	992	0.68	2.56	43	1.63	0.51

d_{100}, d-spacing value; a_o, unit cell parameter; S_{BET}, BET specific surface area; V_p, total pore volume; D_p, average pore diameter (BJH method); C_{BET}, BET constant; W_t, pore wall-thickness.

In respect to the N_2 adsorption-desorption isotherms obtained at 77 K, the profiles for purely siliceous and Al-containing samples corresponded to type IV (in the IUPAC classification), which is typical of the MCM-41 mesoporous molecular sieves with well-defined and ordered cylindrical mesopores[1-3]. The isotherms did not change their shape with the variation of Al content in the samples and in each one three well-defined stages were identified: (*i*) at low relative pressures ($P/P_0 < 0.25$) the N_2 uptake slowly increased attributed to the monolayer-multilayer adsorption on the pore walls; (*ii*) at intermediate relative pressures ($0,25 < P/P_0 < 0.40$) a sharp inflection emerged possibly due to capillary condensation within of small pores, called primary mesopores; and, (*iii*) at high relative pressures ($P/P_0 > 0.4$) a plateau with a slight inclination was observed and assigned to multilayer adsorption of N_2 molecules on the external surface of the crystals. In this work, at relative pressures in the range of 0.4 - 0.9, no perceptible hysteresis loop was detected as it is found in some MCM-41 type mesoporous materials prepared with low surfactant/silicon molar ratios (e.g., CTAB/TEOS ≤ 0.08)[23] or in prolonged post-synthesis hydrothermal treatments at high temperatures (e.g., 4-6 days, 423 K)[12].

The purely siliceous MCM-41 showed a high specific BET surface area (1412 $m^2 g^{-1}$). However, when the Al was incorporated into MCM-41 structure, the specific BET surface area of the solids decreased with the increase of Al loading in the following order: MCM-41 > Al-MCM-41(50) > Al-MCM-41(15). Concomitantly, the BET C constants decrease with Al incorporation from 59 for purely siliceous MCM-41 to 43 for Al-MCM-41(15). These values are within the range of 22 - 134 reported in the literature[8,10]. The BET C constant is related to the N_2 adsorption heat ($Q_{ads} = RT \ln C$) in the first layer[24]. This would be an indication that N_2 molecules adsorb more strongly on MCM-41 silica surfaces than the ones on Al-containing samples. Though, this last may also have been due to the changes of the three-dimensional structure of the purely siliceous MCM-41 with the introduction of Al ions. Notwithstanding, all solids maintained a uniform and unimodal pore size distribution as shown in Figure 2. The total pore volume (0.68 - 1.06 $cm^3 g^{-1}$) and the average pore diameter (2.56 - 2.65 nm) are consistent with the physical nature of the MCM-41 and Al-MCM-41 mesoporous molecular sieves[11,13].

In addition, the pore wall-thickness (W_t) increased from 1.37 to 1.63 nm with the increase of Al content. The latter is in accordance with the increase of the interplanar spacing and of the cell parameter size of the MCM-41 silica (observed by XRD) after the incorporation of Al into its crystalline structure. According to Kurdyukov *et al*.[8] in solids synthesized by non-hydrothermal methods in an alkali-free system, the high BET surface area not only depends on the cylindrical mesopores, but also on the formation of micropores (Dp < 2 nm) within the walls and between the outer surfaces of the ordered silica channels. The latter could be an indicative that the mesoporous materials obtained by non-hydrothermal methods may be fragile. However, the range of pore wall-thickness obtained in this work (1.37 - 1.63 nm) is within the range of those obtained for most solids synthesized by hydrothermal methods (0.84 - 1.66 nm) independent of the type of basic medium used (Table 1). Exceptionally, the high pore wall-thickness (1.92 - 2.35 nm) obtained by Liu *et al*.[16] through hydrothermal methods in sodium ions medium was due to the use of a lower surfactant/silicon ratio (CTAB/TEOS ≈ 0.1). According to Chen *et al*.[23], solids synthesized with lower surfactant/silicon ratios (CTAB/TEOS ≤ 0.1) shows a high pore wall-thicknesses.

TEM images with EDS graphs inset of the MCM-41 and Al-MCM-41 samples are depicted in Figure 3. For all samples, the images exhibit well-ordered channel arrays in unidirectional and parallel straights with very slight degradation of the structure for the Al-containing samples. The latter may be due to the appearance of aluminum-rich dense phases as observed by others authors in samples with $Si/Al \approx 20 - 12$[25]. The EDS graphs confirm the presence of the O, Si and Al elements in the mesoporous samples. These results are consistent with the chemical, low-angle XRD and N_2 adsorption analysis and suggest that the Al-containing samples, after calcination at 813 K, retain the characteristics of regular and hexagonal pore arrangement of MCM-41 type mesoporous materials.

In Figure 4 are shown the ^{29}Si MAS-NMR and ^{27}Al MAS-NMR spectra. The ^{29}Si MAS-NMR resonance of the MCM-41 has two peaks, one intense at -100 ppm due to Q3 structural units, $Si[(OSi)_3(OH)]$, and another at -91 ppm related to Q2 structural units, $Si[(OSi)_2(OH)_2]$. Furthermore, it was also observed a shoulder at -110 ppm which is found only on purely siliceous structures, being attributed to Q4 structural units, $Si[(OSi)_4]$[26,27]. Similarly, the ^{29}Si MAS-NMR spectra of solids Al-MCM-41(50) and Al-MCM-41(15) showed two peaks, one intense at -99 ppm due to the presence of Si species, finding in their neighborhoods an aluminum atom, $Si[(OSi)_3(OAl)]$, and other with low intensity at -90 ppm due to the Si species with two or three aluminum neighboring atoms, $Si[(OSi)_2(OAl)_2]$ and $Si[(OSi)(OAl)_3]$, respectively[18,22,28-30]. In these last two ^{29}Si MAS-NMR resonance profiles, the corresponding peak at -110 ppm was decreasing with the increase the concentration of Al, indicating that aluminosilicates (Al-MCM-41) were formed.

The spectra of ^{27}Al MAS-NMR shows the Al coordination state of Al-MCM-41(50) and Al-MCM-41(15) samples. In both solids the NMR peaks were observed, one with high intensity at 53 ppm assigned to four-coordinated Al species (tetrahedral structures) which may generate the acid sites, and an additional of minor intensity at 0 ppm corresponding to six-coordinated Al species (octahedral structures) which has less contribution to the acidity[18,31]. In this study was observed a broad peak at 53 ppm (Al four-coordinated) decreases and the

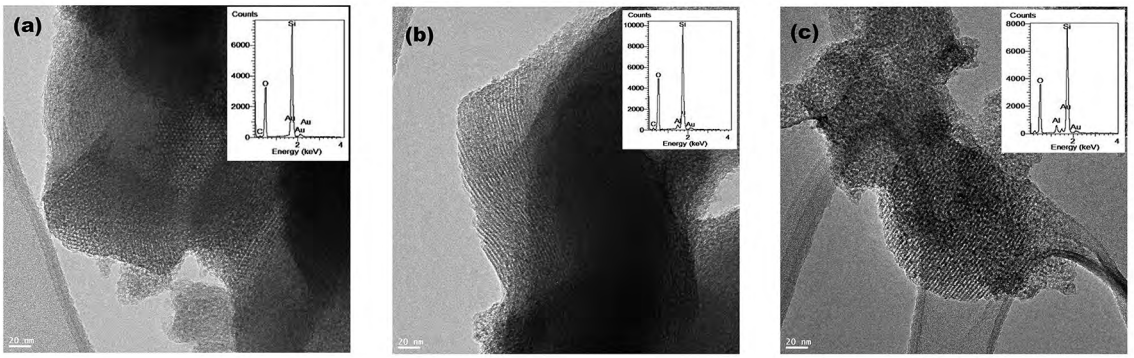

Figure 3. TEM images (× 20nm) and EDS graphs of **(a)** MCM-41; **(b)** Al-MCM-41(50); **(c)** Al-MCM-41(15).

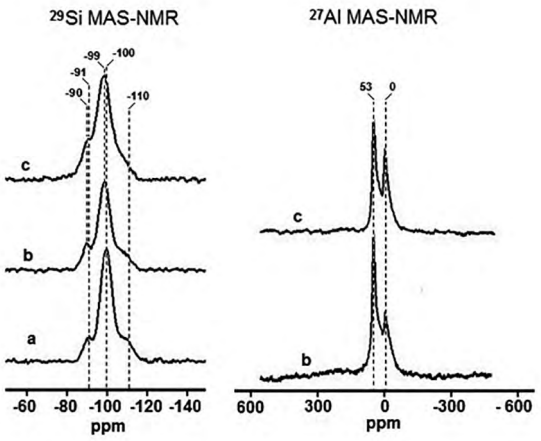

Figure 4. ^{29}Si-NMR and ^{27}Al-NMR spectra of **(a)** MCM-41, **(b)** Al-MCM-41(50), **(c)** Al-MCM-41(15).

line at 0 ppm (Al six-coordinated) increases with increasing aluminum content. On the other hand, the broadening of the peaks at 53 ppm suggests the presence of Al species in highly distorted tetrahedral structures[32]. Furthermore, it is believed when the material is subjected to heat treatment to remove the template surfactant (CTAB), a part of aluminum incorporated into the network coordination site undergoes a change probably caused by the breaking of Si-O-Al bonds, producing species of Al extra-framework or amorphous alumina occluded in the pores, making it a material with a low uniformity degree, without significantly changing the pore structure of the molecular sieve[30]. Nevertheless, the high intensity of the peaks ^{27}Al MAS-NMR at 53 and 0 ppm is also an indicative that the aluminum is present in the samples, mostly forming four-coordinated Al species, and in a less extent, forming six-coordinated Al species, which means that the aluminum atoms were actually incorporated into the silica network by non-hydrothermal methods at room temperature as achieved through direct hydrothermal synthesis[5].

In regard to the acid properties of the mesoporous samples (Table 2), the amount of desorbed NH_3 from pure siliceous MCM-41 exhibited a total acidity of one order of magnitude smaller than that obtained with Al-MCM-41(50) and Al-MCM-41(15)[33-35]. The reduced acidity of the pure siliceous MCM-41 may be attributed to the presence of Si-OH groups in its surface from adsorbed water molecules[26,36-38]. However, when the Si/Al ratio was varied from MCM-41(50) to MCM-41(15), there was not a significant increase in the total acidity in this last sample. The reason might be that the high incorporated aluminum content causes the formation and aggregation of six-coordinated Al species, as was verified by ^{27}Al MAS-NMR, which are responsible by decreasing the density of acid sites[22].

In Figure 5 is shown the FT-IR samples profiles as-synthesized (not calcined) and after calcined in synthetic air stream at 813 K, corresponding to siliceous pure MCM-41 and Al-containing samples like Al-MCM-41(50) and Al-MCM-41(15). In as-synthesized samples were observed bands at 2921, 2852, 1477 and 719 cm^{-1} corresponding to the deformation vibration of the C-H bonds present in the CH_2 and CH_3 groups of the surfactant molecules, CTAB, used as pore template agent[25,26,35,39]. After calcination, those bands disappear completely, indicating that the CTAB molecules were completely removed from the pores of the molecular sieves.

In the after calcined samples, the broad band around 3438 cm^{-1} and the small one at 1630 cm^{-1} are attributed to OH^- groups from adsorbed water molecules[36,31,35,37]. The adsorption bands noticed at 1224 and 1076 cm^{-1} correspond to external and internal asymmetric stretching vibrations of Si-O-Si bonds, respectively, and the band at 798 cm^{-1} is linked to symmetric bending vibrations of Si-O-Si[17,35,40]. According to Basumatary *et al.*[36], the band close to 795 cm^{-1} is characteristic of Si free. Thus, in this work the intensity of the band at 798 cm^{-1} for pure siliceous MCM-41 was higher and decreased with increasing Al content in the MCM-41.

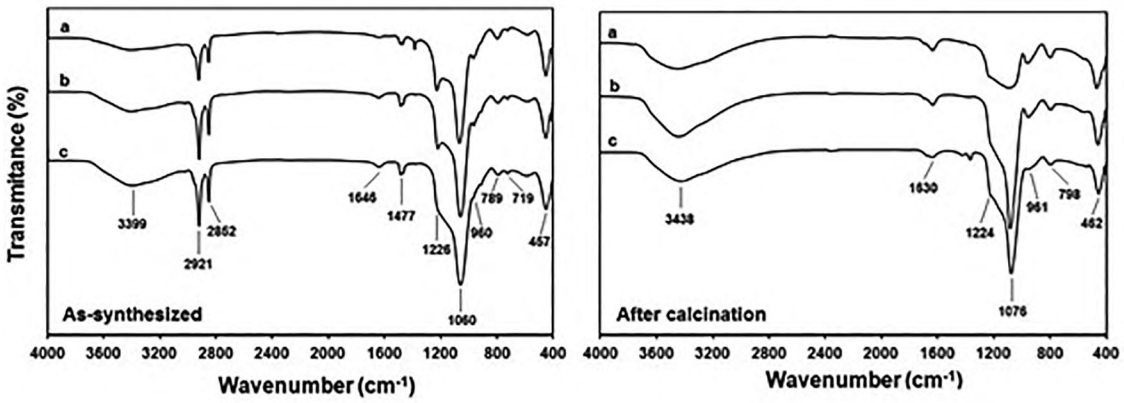

Figure 5. Infrared spectra of the samples of **(a)** MCM-41, **(b)** Al-MCM-41(50), **(c)** Al-MCM-41(15).

Other bands around 462 and 961 cm^{-1} are attributed to tetrahedral bending of Si-O bonds and stretching vibrations of the Si-OH bonds, respectively[17,26,35]. Some authors suggest that the band around 961 cm^{-1} also correspond to the incorporation of heteroatoms into the framework of the mesoporous silica materials, Si-O-M^+ (where M = Al)[17,38]. However, here was observed that the intensity of the band decreased by increasing Al concentration. Apparently, this behavior may indicate the presence of Al extra-framework or as pointed out by ^{27}Al MAS-NMR may be due to the presence of Al species in highly distorted tetrahedral structures.

The thermogravimetric analysis (TGA) profiles and their respective differential thermogravimetric (DTG) analysis of MCM-41, Al-MCM-41(50) and Al-MCM-41(15) samples as-synthesized are shown in Figure 6. The thermal analysis curves show three stages of weight loss as a function of temperature increase. Between temperatures of 300 to 400 K, the weight loss in the range of 2-4% was associated to desorption of physisorbed water on the external surface and removal of water occluded in the mesopores; at 400-650 K the weight loss (33-42%) was related to the oxidative decomposition and removal of organic species from surfactant and organosilica precursors; above 650 K the mass loss (2-7%) was attributed to the oxidation of remaining carbonaceous species as well as the loss of water from the condensation of adjacent silanol groups (Si-OH) to form siloxane bonds (Si-O-Si). Above the calcination temperature (> 813 K), there was no significant weight loss, suggesting that the surfactant template had been removed completely. The DTG curves of all samples showed a peak near 320 K that correspond to first stage of weight loss and two peaks at 530 and 585 K that correspond to second stage. In this work, all peaks did not show significant change in their position with respect to temperature. However, their intensities decreased slightly with Al loading. The latter suggests that the variation of mass loss with respect to variation of temperature (%w/K) is lower for Al-containing solids than the ones for purely siliceous. These results are in agreement with those found in the literature. Thereby, according to Beck *et al.*[1], the organic cations interact much stronger with the Al species than with SiO^- groups.

4. Conclusions

The influence of the aluminum incorporation in the textural properties, crystalline structure and nature of the surface activity of MCM-41 mesoporous structure synthesized by non-hydrothermal method at room temperature and short reaction time in an alkali-free system has been investigated. We used a favorable procedure by which MCM-41, Al-MCM-41(50) and Al-MCM-41(15) mesoporous materials were obtained with high specific BET surface areas in the range of 1000-1400 m^2g^{-1} with the purely siliceous MCM-41 showing the highest surface area. All mesoporous solids showed a well-defined hexagonally ordered pore geometry maintaining a uniform and unimodal pore size distribution. As verified by ^{27}Al MAS-NMR spectrometry the Al^{+3} ions were introduced successfully in the structure of the purely siliceous MCM-41 forming four-coordinated Al species, and in a less extent, forming six-coordinated Al species. These results were corroborated by XRD observations, where the unit cell parameter expanded with the increase of Al content. In addition, the surface acidity of the MCM-41 based materials synthesized increased with Al loading. However, the presence of Al in the MCM-41 mesoporous structure resulted in a decrease on crystallinity and surface area possibly due to the presence of Al species in highly distorted tetrahedral structures and Al extra-framework or amorphous alumina occluded in the pores. In summary, the MCM-41 and Al-MCM-41 molecular sieves have been successfully prepared by non-hydrothermal method in an alkali-free system and showed similar characteristics of those synthesized by hydrothermal method.

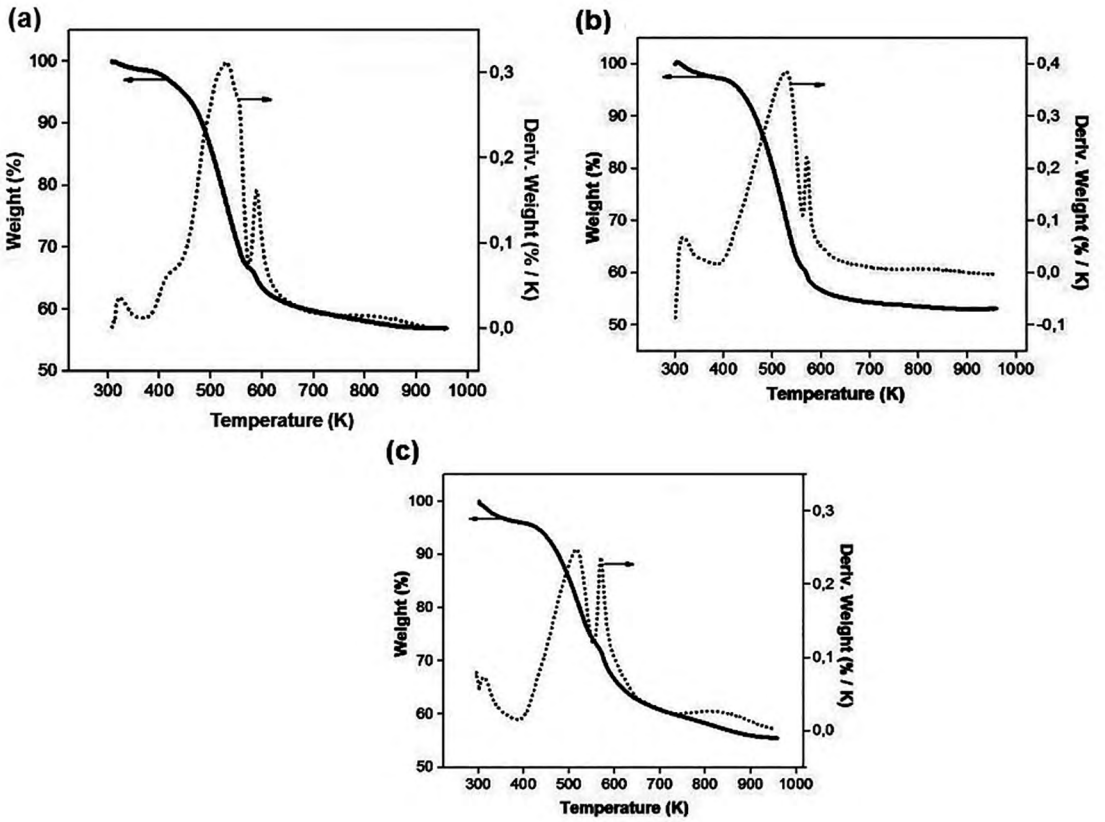

Figure 6. TGA and DTG profiles as-synthesized of **(a)** MCM-41, **(b)** Al-MCM-41(50), **(c)** Al-MCM-41(15).

5. Acknowledgments

This research was supported by the Brazilian funding support agency: CNPq and CAPES (Ciências sem Fronteiras). We are grateful for the financial support.

6. References

1. Beck JS, Vartuli JC, Roth JW, Leonowicz ME, Kresge CT, Schmitt KD, et al. A new family of mesoporous molecular sieves prepared with liquid crystal templates. *Journal of the American Chemical Society* 1992;114(27):10834-10843.

2. Kresge CT, Leonowicz ME, Roth WJ, Vartuli JC, Beck JS. Ordered mesoporous molecular sieves synthesized by a liquid-crystal template mechanism. *Nature*1992;359:710-712.

3. Chen CY, Li HL, Davis ME. Studies on mesoporous materials: I. Synthesis and characterization of MCM-41. *Microporous Materials*1993;2(1):17-26.

4. Corma A. From Microporous to Mesoporous Molecular Sieve Materials and Their Use in Catalysis. *Chemical Reviews* 1997;97(6):2373-2420.

5. Zhao XS, Lu GQ, Millar GJ. Advances in Mesoporous Molecular Sieve MCM-41. *Industrial & Engineering Chemistry Research* 1996;35(7):2075-2090.

6. Tuel A. Modification of mesoporous silicas by incorporation of heteroelements in the framework. *Microporous and Mesoporous Materials*1999;27(2-3):151-169.

7. Pauly TR, Petkov V, Liu Y, Billinge SJL, Pinnavaia TJ. Role of Framework Sodium versus Local Framework Structure in Determining the Hydrothermal Stability of MCM-41 Mesostructures. *Journal of the American Chemical Society*2002;124(1):97-103.

8. Kurdyukov DA, Eurov DA, Kirilenko DA, Kukushkina JA, Sokolov VV, Yagovkina MA, et al. High-surface area spherical micro-mesoporous silica particles. *Microporous and Mesoporous Materials* 2016;223:225-229.

9. Matsumoto A, Chen H, Tsutsumi K, Grün M, Unger K. Novel route in the synthesis of MCM-41 containing framework aluminum and its characterization. *Microporous and Mesoporous Materials* 1999;32(1-2):55-62.

10. Ribeiro-Carrott MML, Conceição FL, Lopes JM, Carrott PJM, Bernardes C, Rocha J, et al. Comparative study of Al-MCM materials prepared at room temperature with different aluminium sources and by some hydrothermal methods. *Microporous and Mesoporous Materials* 2006;92(1-3):270-285.

11. Tayade KN, Mishra M. Catalytic activity of MCM-41 and Al grafted MCM-41 for oxidative self and cross coupling of amines. *Journal of Molecular Catalysis A: Chemical*2014;382:114-125.

12. Sayari A, Liu P, Kruk M, Jaroniec M. Characterization of Large-Pore MCM-41 Molecular Sieves Obtained via Hydrothermal Restructuring. *Chemistry of Materials* 1997;9(11):2499-2506.

13. Brahmi L, Ali-Dahmane T, Hamacha R, Hacini S. Catalytic Performance of Al-MCM-41 Catalyst for the Allylation of Aromatic Aldehydes with Allyltrimethylsilane: Comparison with $TiCl_4$ as Lewis acid. *Journal of Molecular Catalysis A: Chemical* 2016;423:31-40.

14. Qin J, Li B, Zhang W, Lv W, Han C, Liu J. Synthesis, characterization and catalytic performance of well-ordered mesoporous Ni-MCM-41 with high nickel content. *Microporous and Mesoporous Materials* 2015;208:181-187.

15. Zhao XS, Lu GQ, Millar GJ, Li SX. Synthesis and characterization of highly ordered MCM-41 in an alkali-free system and its catalytic activity. *Catalysis Letters*1996;38(1-2):33-37.

16. Liu X, Sun H, Yang Y. Rapid synthesis of highly ordered Si-MCM-41. *Journal of Colloid and Interface Science* 2008;319(1):377-380.

17. Vaschetto EV, Monti GA, Herrero ER, Casuscelli SG, Eimer GA. Influence of the synthesis conditions on the physicochemical properties and acidity of Al-MCM-41 as catalysts for the cyclohexanone oxime rearrangement. *Applied Catalysis A: General* 2013;453:391-402.

18. Reddy KM, Song C. Synthesis of mesoporous molecular sieves: influence of aluminum source on Al incorporation in MCM-41. *Catalysis Letters*1996;36(1-2):103-109.

19. Vaschetto EG, Pecchi GA, Casuscelli SG, Eimer GA. Nature of the active sites in Al-MCM-41 nano-structured catalysts for the selective rearrangement of cyclohexanone oxime toward ?-caprolactam. *Microporous and Mesoporous Materials*2014;200:110-116.

20. La-Salvia N, Lovón-Quintana JJ, Valença GP. Vapor-phase catalytic conversion of ethanol into 1,3-butadiene on Cr-Ba/MCM-41 catalysts. *Brazilian Journal of Chemical Engineering* 2015;32(2):489-500.

21. Borade RB, Clearfield A. Synthesis of aluminum rich MCM-41. *Catalysis Letters*1995;31(2-3):267-272.

22. Luan Z, Cheng CF, Zhou W, Klinowsk J. Mesopore Molecular Sieve MCM-41 Containing Framework Aluminum. *The Journal of Physical Chemistry*1995;99(3):1018-1024.

23. Chen H, Wang Y. Preparation of MCM-41 with high thermal stability and complementary textural porosity. *Ceramics International* 2002;28(5):541-547.

24. Zhao XS, Lu GQ, Whittaker AK, Millar GJ, Zhu HY. Comprehensive Study of Surface Chemistry of MCM-41 Using ^{29}Si CP/MAS NMR, FTIR, Pyridine-TPD, and TGA. *The Journal of Physical Chemistry B* 1997;101(33):6525-6531.

25. Kloetstra KR, Zandbergen HW, van Bekkum H. MCM-41 type materials with low Si/A1 ratios. *Catalysis Letters* 1995;33(1-2):157-163.

26. Yasmin T, Müller K. Structural characterization of alkyl bonded MCM-41 silica materials prepared by supercritical fluid approach. *Microporous and Mesoporous Materials* 2015;208:83-92.

27. Liu M, Hou L, Yu S, Xi B, Zhao Y, Xia X. MCM-41 impregnated with A zeolite precursor: Synthesis, characterization and tetracycline antibiotics removal from aqueous solution. *Chemical Engineering Journal* 2013;223:678-687.

28. Murata K, Liu Y, Inaba M, Mimura N. Effect of Ti-modified mesoporous materials on the direct epoxidation of propylene by molecular oxygen. *Catalysis Today*2004;91-92:39-42.

29. Dedecek J, Sklenak S, Li C, Wichterlová B, Gábová V, Brus J, et al. Effect of Al-Si-Al and Al-Si-Si-Al Pairs in the ZSM-5 Zeolite Framework on the ^{27}Al NMR Spectra. A Combined High-Resolution ^{27}Al NMR and DFT/MM Study. *The Journal of Physical Chemistry C* 2009;113(4):1447-1458.

30. Melo RAA, Giotto MV, Rocha J, Urquieta-González EA. MCM-41 Ordered Mesoporous Molecular Sieves Synthesis and Characterization. *Materials Research*1999;2(3):173-179.

31. Li Q, Wu Z, Tu B, Park SS, Ha CS, Zhao D. Highly hydrothermal stability of ordered mesoporous aluminosilicates Al-SBA-15 with high Si/Al ratio. *Microporous and Mesoporous Materials* 2010;135(1-3):95-104.

32. Occelli ML, Biz S, Auroux A, Ray GJ. Effects of the nature of the aluminum source on the acidic properties of some mesostructured materials. *Microporous and Mesoporous Materials* 1998;26(1-3):193-213.

33. González F, Pesquera C, Perdigón A, Blanco C. Synthesis, characterization and catalytic performance of Al-MCM-41 mesoporous materials. *Applied Surface Science* 2009;255(17):7825-7830.

34. Iwanami K, Sakakura T, Yasuda H. Efficient catalysis of mesoporous Al-MCM-41 for Mukaiyama aldol reactions. *Catalysis Communications*2009;10(15):1990-1994.

35. Rosenholm JB, Rahiala H, Puputti J, Stathopoulos V, Pomonis P, Beurroies I, et al. Characterization of Al and Ti-modified MCM-41 using adsorption techniques. *Colloids and Surfaces A: Physicochemical and Engineering Aspects*2004;250(1-3):289-306.

36. Basumatary AK, Kumar RV, Ghoshal AK, Pugazhenthi G. Synthesis and characterization of MCM-41-ceramic composite membrane for the separation of chromic acid from aqueous solution. *Journal of Membrane Science*2015;475:521-532.

37. Roik NV, Belyakova LA. Sol-gel synthesis of MCM-41silicas and selective vapor-phase modification of their surface. *Journal of Solid State Chemistry*2013;207:194-202.

38. Pradhan AC, Martha S, Mahanta SK, Parida KM. Mesoporous nanocomposite Fe/Al_2O_3 MCM-41: An efficient photocatalyst for hydrogen production under visible light. *International Journal of Hydrogen Energy*2011;36(20):12753-12760.

39. Shibata H, Chiba Y, Kineri T, Matsumoto M, Nishio K. The effect of heat treatment on the interplanar spacing of the mesostructure during the synthesis of mesoporous MCM-41 silica. *Colloids and Surfaces A: Physicochemical and Engineering Aspects* 2010;358(1-3):1-5.

40. Li Z, Gao L, Zheng S. SEM, XPS, and FTIR studies of MoO_3 dispersion on mesoporous silicate MCM-41 by calcination. *Materials Letters*2003;57(29):4605-4610.